



ELSEVIER

Contents lists available at [SciVerse ScienceDirect](http://SciVerse.ScienceDirect.com)

Physica E

journal homepage: www.elsevier.com/locate/physa

The influence of annealing on structural and photoluminescence properties of silicon-rich Al₂O₃ films prepared by co-sputtering

N. Korsunskaya^a, T. Stara^a, V. Strelchuk^a, O. Kolomys^a, V. Kladko^a, A. Kuchuk^a, L. Khomenkova^{b,*}, J. Jedrzejewski^c, I. Balberg^c

^a V. Lashkaryov Institute of Semiconductor Physics, 45 Pr. Nauky, 03028 Kyiv, Ukraine

^b CIMAP/Ensicaen, 6 Boulevard Marechal Juin, 14050 Caen, France

^c Racah Institute of Physics, Hebrew University, 91904 Jerusalem, Israel

HIGHLIGHTS

- ▶ Si-rich Al₂O₃ films with different Si content were fabricated by RF magnetron sputtering.
- ▶ Their structural and luminescence properties were studied versus thermal treatment.
- ▶ Amorphous Si clusters were formed during deposition in the films with high Si content.
- ▶ High-temperature annealing leads to the formation of Si nanocrystals emitted at ~850 nm.
- ▶ Si nanocrystals act as efficient sensitizers of different radiative host defects.

ARTICLE INFO

Article history:

Received 16 November 2012

Received in revised form

30 November 2012

Accepted 6 December 2012

Available online 13 December 2012

ABSTRACT

Si-rich Al₂O₃ films were produced by RF magnetron co-sputtering of pure silicon and alumina targets onto a long silicon oxide substrate. The effect of an annealing treatment on structure and light emission property of the films with different Si content was investigated by means of X-ray diffraction, Raman scattering and photoluminescence (PL) methods. The formation of amorphous Si clusters upon deposition process was observed for the films with Si volume content exceeded 70%. The annealing treatment of the films with Si content exceeded 80% results in the formation of Si crystallites with the mean size of about ~14 nm. Three overlapped PL bands were detected in the 500–950 nm spectral range. The analysis of PL spectrum shape revealed that the near-infrared PL component, peaked at 850 nm, is caused by the exciton recombination inside Si crystallites. Another, the most intense PL band with maximum at 560–580 nm can be ascribed to defects in matrix located near nanocrystal/matrix interface, while the origin of the third PL band with the peak position at 700–750 nm is supposed to be also due to host defects whose nature requires more investigation.

© 2012 Elsevier B.V. All rights reserved.

1. Introduction

Nowadays, different semiconductor nanostructures offer their wide photonic and microelectronic applications. Among them, silicon nanocrystallites (Si-ncs) attract considerable attention due to a significant transformation of their optical and electrical properties caused by quantum-confinement effect [1–3]. Light-emitting Si-ncs embedded in dielectric host give a hand to the development and implementation of fully Si-based opto- and microelectronic devices.

Silicon oxide is the most considered host for Si-ncs. During last decades, numerous investigations of the Si-ncs-SiO₂ systems brought many promising results [3–9]. It was found that bright luminescence in wide spectral range at room temperature originates from recombination of excitons in quantum confinement Si-ncs; the variation of their sizes allows tuning of emission wavelength from the blue to the near-infrared range [3–7]. Besides this attractive photoluminescence property, Si-ncs-SiO₂ nanostructures were proposed for new generation of solar cells [8]. Furthermore, Si-ncs embedded in dielectric matrix have regained interest as a candidate for non-volatile memory applications because of higher performance of devices [9–11]. However, because of aggressive down-scaling of microelectronic devices the SiO₂ met its limit as a gate material due to high leakage current. In this regard, other dielectrics as ZrO₂, HfO₂, Al₂O₃, etc. became more addressed [12–14].

* Corresponding author. Tel.: +33231452671.

E-mail addresses: larysa.khomenkova@ensicaen.fr, khomenkova@rambler.ru (L. Khomenkova).

From photonic application viewpoint, Al_2O_3 is more interesting host material for optical communication in comparison with SiO_2 . Along with similar bandgap energy, it has higher refractive index (1.73 at 1.95 eV) than that of SiO_2 (1.46 at 1.95 eV) and allows better light confinement, making compact device structures possible. Promising properties of alumina-based waveguides with embedded Si-ncs and Er^{3+} ions offered an enhancement of the Er^{3+} emission due to higher solubility of Er^{3+} ions in alumina host [15–19]. However, in spite of promising properties, Si-ncs- Al_2O_3 materials were not well addressed.

Several approaches have been used to form Si-ncs in amorphous and/or crystalline Al_2O_3 . The most known methods are Si ion implantation [20], laser ablation [21] and electron beam evaporation followed by subsequent high-temperature annealing. For these systems the successful formation of Si-ncs was already demonstrated. However, in spite of simplicity of magnetron co-sputtering approach and its wide application for the fabrication of Si-rich- SiO_2 materials [4,8,12], only few groups applied this method for deposition of Si-rich-alumina [21–23]. In this work, the Si-rich- Al_2O_3 layers with different Si content were fabricated by magnetron co-sputtering and the effect of annealing treatment on structural and luminescent properties was investigated.

2. Experimental techniques

The Si-rich- Al_2O_3 films were deposited by radio frequency magnetron co-sputtering of two spaced-apart targets (pure Si and Al_2O_3) in pure argon plasma on a long silicon oxide substrate (Fig. 1a). The length and the width of this substrate were 6 in. and 0.5 in., respectively. Before deposition, both the substrate and the template were submitted to standard RCA cleaning procedure, dried in nitrogen and placed in a load-lock chamber of the deposition unit. The background vacuum in a main chamber was about 1×10^{-5} Pa prior to the deposition. The distance between the targets and the substrate was fixed at 64 mm. The RF power applied to Si and Al_2O_3 targets (2 in. in diameter) were 40 W and 80 W, respectively. The deposition was performed at room temperature during 250 min.

The film was grown on non-rotated long substrate. We used this approach in our previous works for fabrication of Si-rich- SiO_2 films by simultaneous sputtering of Si and SiO_2 targets [4]. It

permitted to obtain the film with varied excess Si content along the film during one deposition run at fixed powers applied to the targets. An annealing treatment of such long film gives the possibility to investigate simultaneously the formation of the Si-ncs in the films with different Si excess.

In the present work, the use of the long substrate with the template (Fig. 1) allowed depositing of the Si-rich- Al_2O_3 films with a 4 mm width and a 140 mm length. The film thickness was in the range 1000–1300 nm for different points, demonstrating a trend to increase towards Si-rich-side. The variation of the Si content volume along the film length (C_{Si}) was estimated in the next way. Besides the Si-rich- Al_2O_3 film, another Si layer was grown at the same conditions from Si target only (Fig. 1b). Then, the C_{Si} value was determined as $C_{\text{Si}} = V_{\text{Si}} / V_{\text{Si-Al}_2\text{O}_3}$, where V_{Si} and $V_{\text{Si-Al}_2\text{O}_3}$ are the volumes of pure Si and Si-rich- Al_2O_3 films, respectively, measured in the corresponding points. Considering the equal width for both layers, the ratio of volumes corresponds to the ratio of thicknesses determined in corresponding points. The C_{Si} values obtained in this way varied from 22 vol% (Si-poor side) to 98 vol% (Si-rich side).

To form Si-ncs in alumina host, the long samples were submitted to a conventional annealing in a horizontal furnace at 1150 °C during 30 min in nitrogen flow. After this, they were cut into smaller (1 cm in the length) pieces (called hereafter as samples) to simplify the investigation of their properties.

The microstructure and photoluminescence (PL) of the samples were investigated. X-ray diffraction (XRD) study was carried out using Philips X'Pert-MRD diffractometer with Cu $K\alpha$ -radiation ($\lambda = 0.15406$ nm) in a grazing geometry (angle of incidence was 5°). The micro-Raman characterization was performed in 100–900 cm^{-1} spectral range by means of a Horiba Jobin-Yvon T-64000 Raman spectrometer equipped with confocal microscope and automated piezo-driven XYZ stage. An Ar–Kr ion laser was used as excitation source. The laser power on the sample surface was always kept below 5 mW to obtain the best signal-to-noise ratio, preventing a laser heating of sample investigated. The spectral resolution of the spectrometer was less than 0.15 cm^{-1} . For PL study, an Innova 90C coherent Ar⁺ laser was used as excitation source. The PL spectra were recorded at room temperature using a fast Hamamatsu R5108 photomultiplier tube after dispersion of the light through a Jobin-Yvon TRIAX 180 monochromator linked with a SRS lock-in amplifier (SP830 DPS)

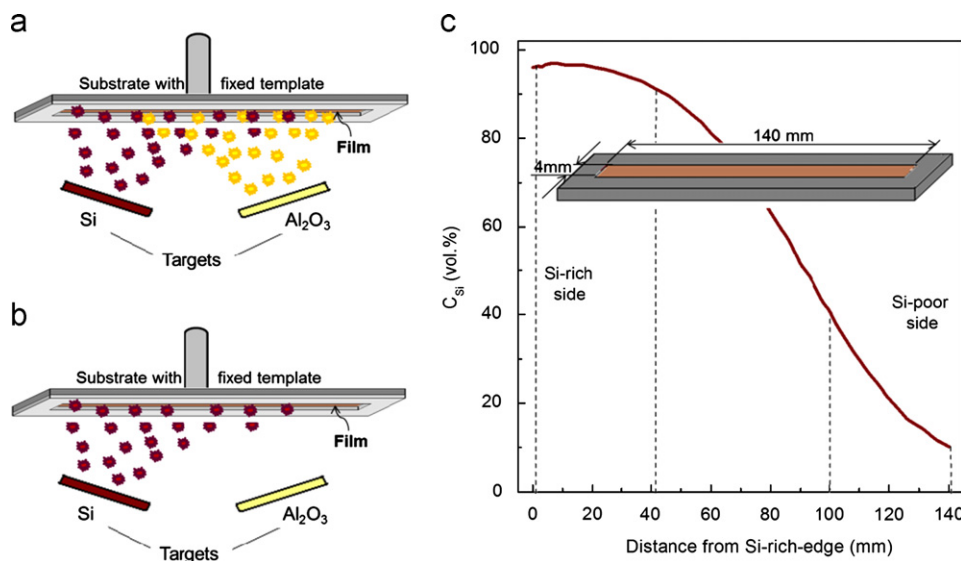


Fig. 1. (a, b) Schematic presentation of the configuration of the deposition process of Si-rich- Al_2O_3 (a) and pure Si film (b). (c) Variation in Si volume excess in the film. Inset – schematic presentation of the film grown on long substrate.

referenced to the chopping frequency of light fixed at 20 Hz. The PL spectra were detected in the 500–1000 nm spectral range using 488 nm excitation light wavelength. All PL spectra were corrected on the spectral response of detection system. The investigations were performed at 300 K.

3. Results and discussion

3.1. Structural properties of the samples

3.1.1. Raman scattering spectra of as-deposited films

First of all, the microstructure of as-deposited films was investigated versus C_{Si} . The micro-Raman (μ -RS) spectra of the samples with $C_{Si} \geq 70\%$ demonstrate two broad bands, centered at $140\text{--}160\text{ cm}^{-1}$ and at $460\text{--}470\text{ cm}^{-1}$ (Fig. 2, curves 1 and 2). The shape of the signal and its spectral range correspond to the signal from amorphous Si. Generally, it can be identified as four bands of Si-related acoustic and optical phonon modes: transverse and longitudinal acoustic (TA and LA) phonons as well as longitudinal and transverse optical (LO and TO) modes. All of them are also shown in Fig. 2. As one can see, the peak position of one of these bands (i.e. the TO band (about 460 cm^{-1})) is shifted towards the lower wavenumbers with the respect to the peak position of TO-phonon observed usually in μ -RS spectra of amorphous Si (at about 480 cm^{-1}). One of the reasons of this shift can be the tensile stress between Si-rich- Al_2O_3 film and SiO_2 substrate due to the mismatching in lattice parameters.

The observation of phonon spectrum of amorphous Si in as-deposited Si-rich- Al_2O_3 films with $C_{Si} \geq 70\%$ (Fig. 1, curves 1 and 2) is the evidence of amorphous silicon clusters' formation during film deposition. When $C_{Si} < 80\%$, the intensity of all Raman signal decreases, TO phonon band broadens as well as the intensities of TA and LA modes increase (Fig. 2, curve 2). This behavior of the spectra is due to decrease in Si cluster sizes which caused a disorder enhancement (Fig. 2, curve 2). An additional band in the $600\text{--}640\text{ cm}^{-1}$ spectral range was observed for all these samples. It corresponds to a- SiO_2 and, although its intensity is very low, one can conclude that SiO_2 phase is also present in the samples with $C_{Si} \geq 70\%$.

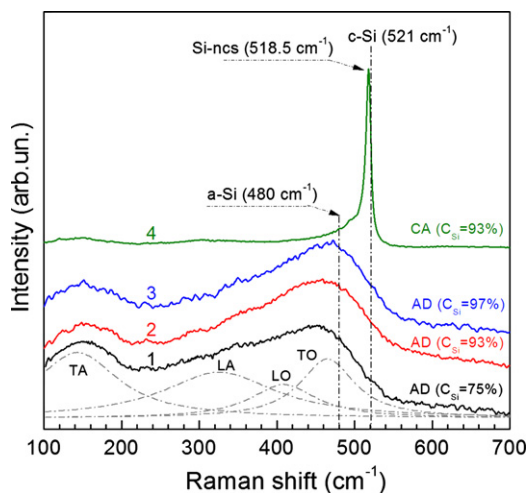


Fig. 2. Micro-Raman scattering spectra of as-deposited (1–3) and annealed (4) of Si-rich- Al_2O_3 films with $C_{Si} = 75\%$ (1), 93 (2,4) and 97% (3). The deconvolution of curve 1 on four Si-phonon bands is present (by dash-dot curves) to demonstrate the shift of TO phonon in as-deposited films in comparison with the peak of amorphous Si.

3.1.2. Raman scattering spectra of annealed films

An annealing of the samples at $1150\text{ }^\circ\text{C}$ during 30 min in nitrogen flow results in the narrowing of TO phonon and its spectral shift towards the higher wavenumbers accompanied by the increase in the intensity. This means that thermal treatment stimulates the formation of Si crystallites, as it is shown, for instance, for samples with $C_{Si} = 93\%$ (Fig. 1, curve 3). However, the peak position of TO phonon demonstrates independence on Si content and it is observed at about to $\sim 518.5\text{ cm}^{-1}$, demonstrating low-frequency shift with respect to TO phonon in bulk Si ($\sim 521\text{ cm}^{-1}$). For the case of low C_{Si} values, it could be caused by quantum confined Si-ncs. However, the same TO peak position detected for annealed samples with high C_{Si} can be rather due to the stress in Si-ncs than the quantum confinement effect. Since this shift for annealed samples occurs toward lower wavenumbers with the respect to TO peak position of intrinsic c-Si (521 cm^{-1}), one can conclude that the Si-ncs are under tensile stress. This latter can be assigned to the tensile stress between Si-rich- Al_2O_3 film and SiO_2 substrate that is in agreement with μ -RS data obtained for as-deposited samples.

It is obvious that the independence of the peak position of TO phonon for annealed samples does not allow correct estimation of the Si-ncs sizes versus Si content. Thus, an additional study of structural properties of the samples was performed by means of X-ray diffraction method.

3.1.3. XRD diffraction study

The information on the Si-ncs sizes was obtained from XRD study. Fig. 3 represents the fragment of XRD pattern corresponded to beam diffraction from Si crystallographic planes at $2\theta \approx 28.4^\circ$ (1 1 1). For the samples with high C_{Si} ($> 80\%$) this peak is pronounced enough (Fig. 3, curves 1 and 2), while for the samples with $C_{Si} \leq 75\%$ it is absent (Fig. 3, curve 3). Moreover, no diffraction peak from crystallized Al_2O_3 was detected. This indicates that the Si-ncs are embedded in amorphous Al_2O_3 matrix.

The mean size of Si-ncs ($\langle d_{Si} \rangle$) was estimated using the Scherrer formula. For the samples with $C_{Si} = 80\text{--}98\%$, $\langle d_{Si} \rangle$ is practically independent on Si content and is equal $\langle d_{Si} \rangle \approx 14\text{ nm}$. The presence of large Si-ncs in these samples can be explained by the formation of the large amorphous Si inclusions during deposition process and their crystallization upon an annealing treatment at $1150\text{ }^\circ\text{C}$. However, it is not excluded the existence of the smaller crystallites in the samples with $C_{Si} = 80\text{--}98\%$. Our recent study showed that evolution of amorphous Si phase is affected by the temperature and duration of annealing treatment. A formation of Si-ncs with $\langle d_{Si} \rangle \approx 5\text{--}6\text{ nm}$ was observed after rapid thermal

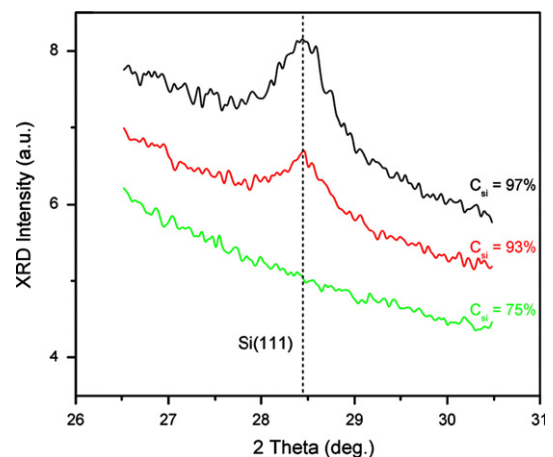


Fig. 3. XRD pattern of Si-rich- Al_2O_3 samples annealed at $1150\text{ }^\circ\text{C}$ during 30 min in nitrogen flow. The vertical dashed line show position of (1 1 1) peak for Si-bulk.

annealing in contrast to the conventional annealing [24]. Besides, the amorphous Si phase was also detected in those samples by Raman scattering method, testifying that the crystallization process was not completed. Longer annealing treatment is required, as it was observed for the samples investigated in the present study.

3.2. Light emitting properties of the samples

3.2.1. As-deposited films

No PL emission was detected for as-deposited samples with $C_{Si} > 75\%$, whereas a weak PL emission in the 500–700 nm spectral range was observed for the films with $C_{Si} < 70\%$ (Fig. 4). The peak position of this PL band is in the 550–570 nm spectral range, demonstrating a slight shift to the shorter wavelengths with C_{Si} increase. The comparison of these PL spectra (Fig. 4, curves 1–3) with the emission detected from quartz substrate (Fig. 4, curve 4) allows to conclude that this visible emission from as-deposited Si-rich- Al_2O_3 films originates from the host defects. These latter can be not only SiO_2 related defects but also Al_2O_3 related centers (such as oxygen vacancies) [5,20].

3.2.2. Annealed films

An annealing treatment causes an appearance of the visible PL emission for the samples with $C_{Si} > 75\%$ (Fig. 5a) and an enhancement of PL emission for other samples (Fig. 5b). As one can see, the PL spectra for the samples with $C_{Si} < 90\%$ consist of two broad PL bands. Their maxima are observed at about 560–580 nm and

about 850 nm for the samples with $C_{Si} = 75\text{--}85\%$ (Fig. 5a) as well as at 560–580 nm and 700–750 nm for the samples with $C_{Si} \leq 70\%$ (Fig. 5b). The last band is accompanied by a long-wavelength tail that can be considered as a presence of near-infrared PL component. Meanwhile, the PL spectrum for the sample with $C_{Si} = 95\%$ (Fig. 5a, curve 1) is represented by one broad band peaked at about 600 nm with a similar long-wavelength tail. It should be noted that PL spectra of the majority of the samples can be approximated by three bands with peak positions in the spectral range 560–580 nm, 700–750 nm and 840–850 nm.

The analysis of PL spectra of annealed samples with different C_{Si} (Fig. 5) shows that when two PL components are well defined in the spectra, the peak positions of visible and near-infrared bands are almost constant. At the same time, the PL intensity of visible band, detected at 560–580 nm, changes slightly for $C_{Si} \approx 85\text{--}95\%$, whereas it increases significantly when C_{Si} decreases to 75–80%, being almost constant for $C_{Si} < 70\%$ (Fig. 6b, curve 2). At the same time, the near-infrared PL component demonstrates a gradual increase in the intensity when the C_{Si} decreases from 95% to 40% that is followed by this PL quenching for the lower C_{Si} values (Fig. 6b, curve 3). It is worth to note that the detection wavelength for this case was about 850 nm to avoid overlapping of near-infrared component with that observed at 700–750 nm (Fig. 5b).

The comparison of XRD and PL data shows that when C_{Si} decreases, the intensity of near-infrared PL band (or component) at first increases and then slightly decreases. This fact can be naturally explained by the changes in the quantity of small Si-ncs followed the C_{Si} decrease. Thus, near-infrared PL component can be ascribed to carrier recombination inside Si-ncs. It should be noted that the band with the same peak position was observed in Si rich Al_2O_3 by other researchers [20] and was also ascribed to carrier recombination inside Si nanocrystals. The visible band at 560–580 nm is similar to the band observed in as-deposited samples and can also be ascribed to carrier recombination through defects in matrix. At the same time its intensity increases sharply with C_{Si} decrease along with the increase in the intensity of near-infrared PL component (Fig. 6b). Because of this, it can be assumed that the defects responsible for this band are located near Si-ncs/matrix interface and the energy transfer from Si-ncs toward these defects occurs. At the same time the dependence of above mentioned band intensity on C_{Si} can also be modified by the increase in defect number. Since this band intensity essentially exceeds the intensity of near-infrared band, one can conclude that the main contribution to the PL spectrum is given by the radiative defects, whereas the Si-ncs play a role of their sensitizers. It is worth to note, that the PL band at 700–750 nm

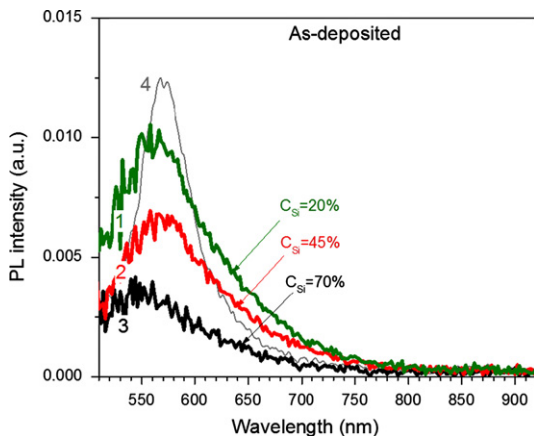


Fig. 4. PL spectra of as-deposited Si-rich- Al_2O_3 samples (1–3) with $C_{Si} = 20\%$ (1), 45 (2) and 70% (3). Curve 4 represents the PL spectrum from quartz substrate.

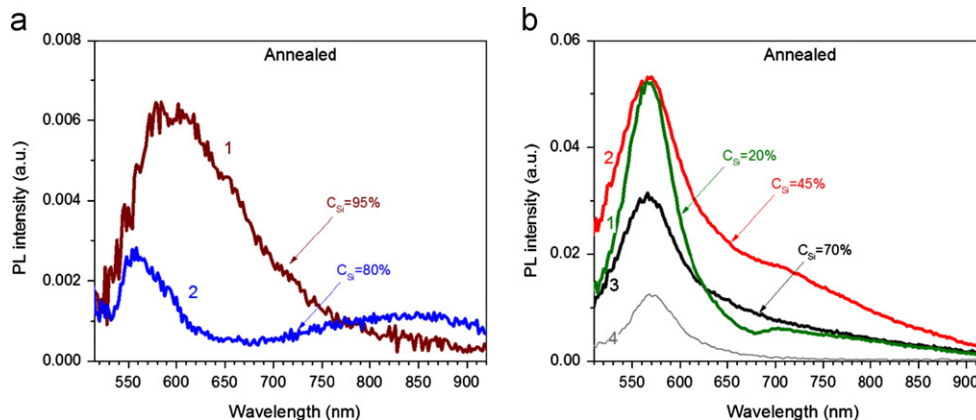


Fig. 5. PL spectra of annealed Si-rich- Al_2O_3 films (a) with $C_{Si} = 95\%$ (1) and 80% (2) and (b) with $C_{Si} = 20\%$ (1), 45 (2) and 70% (3). Curve 4 in Fig. 5(b) corresponds to the PL spectrum from the substrate.

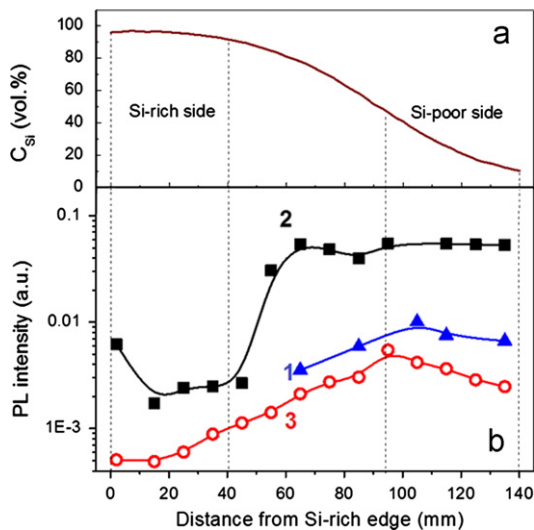


Fig. 6. Variation of the C_{Si} (a) and PL intensity (b) along the Si-rich- Al_2O_3 layer; in figure (b) curve 1 shows the PL intensity of as-deposited sample detected at PL maximum (560–580 nm) accordingly to the spectra presented in Fig. 4; curves 2 and 3 demonstrate the variation of PL intensity detected at 560–580 nm (curve 2) and 850 nm (curve 3).

can be due to host defects. However, their nature requires more investigation.

4. Conclusion

The effect of annealing treatment on structural and light emission properties of Si-rich- Al_2O_3 films with different Si content was investigated. The formation of amorphous Si clusters upon deposition process was observed for the films with Si volume content exceeded 70 vol%. The annealing results in formation of Si crystallites with the mean size of about ~ 14 nm ($C_{Si} > 80\%$). Three broad PL bands were observed in the 500–900 nm spectral range. One of them, near-infrared PL band with peak position ~ 850 nm, is ascribed to the exciton recombination inside Si-ncs. Another one, visible band with peak position at 560–580 nm, is due to radiative recombination via the defects located in the host near crystallite/host interface. The origin of the band with peak position at 700–750 nm is supposed to be also due to defects, whereas its origin needs an additional study.

Acknowledgment

This work was supported by National Academy of Sciences of Ukraine, Ministry of Art and Science of Israel, and National Center for Scientific Research of France.

References

- [1] L.T. Canham, *Applied Physics Letters* 58 (1990) 1057.
- [2] V. Lehman, U. Gosele, *Applied Physics Letters* 61 (1991) 1948.
- [3] T. Shimizu-Iwayama, S. Nakao, K. Saitoh, *Applied Physics Letters* 65 (1994) 1814.
- [4] X.Y. Chen, Y.F. Lu, L.J. Tang, Y.H. Wu, B.J. Cho, X.J. Xu, J.R. Dong, W.D. Song, *Journal of Applied Physics* 97 (2005) 014913.
- [5] L. Khomenkova, N. Korsunskaya, V. Yukhimchuk, B. Jumaev, T. Torchinska, A. Vivas Hernandez, A. Many, Y. Goldstein, E. Savir, J. Jedrzejewski, *Journal of Luminescence* 102/103 (2003) 705.
- [6] G.G. Qin, X.S. Liu, S.Y. Ma, J. Lin, G.Q. Yao, X.Y. Lin, K.X. Lin, *Physical Review B* 55 (1997) 12876.
- [7] T.V. Torchynska, V. Vorobiev (Eds.), *Nanocrystals and Quantum Dots of Group IV Semiconductors*, American Scientific Publishers, California, USA, 2010.
- [8] M.A. Green, *Third Generation Photovoltaics*, B. Springer, Heidelberg, 2006 160 p.
- [9] Z. Lu, J. Shen, B. Mereu, M. Alexe, R. Scholz, V. Talalaev, M. Zacharias, *Applied Physics A: Materials Science & Processing* 80 (2005) 1631.
- [10] R.F. Steimle, R. Muralidhar, R. Rao, *Microelectronics Reliability* 47 (2007) 585.
- [11] T. Baron, A. Fernandes, J.F. Damlencourt, B. De Salvo, F. Martin, F. Mazen, S. Hauka, *Applied Physics Letters* 82 (2003) 4151.
- [12] L. Larcher, A. Padovani, *Microelectronics Reliability* 50 (2010) 1251.
- [13] L. Khomenkova, X. Portier, J. Cardin, F. Gourbilleau, *Nanotechnology* 21 (2010) 285707.
- [14] G. He, L.Q. Zhu, Z.Q. Sun, Q. Wan, L.D. Zhang, *Progress in Materials Science* 56 (2011) 475.
- [15] G.D. Wilk, R.M. Wallace, J.M. Anthony, *Journal of Applied Physics* 89 (2001) 5243.
- [16] G.N. van den Hoven, E. Snoeks, A. Polman, J.W.M. van Uffelen, Y.S. Oei, M.K. Smit, *Applied Physics Letters* 62 (1993) 3065.
- [17] M.K. Smit, G.A. Acket, C.J. van der Laan, *Thin Solid Films* 138 (1986) 171.
- [18] G.N. van den Hoven, R.J.I.M. Koper, A. Polman, C. van Dam, J.W.M. van Uffelen, M.K. Smit, *Applied Physics Letters* 68 (1996) 1886.
- [19] R. Serna, C.N. Afonso, *Applied Physics Letters* 69 (1996) 1541.
- [20] A.N. Mikhaylov, A.I. Belov, A.B. Kostyuk, I. Yu., D.S. Zhavoronkov, A.V. Korolev, A.V. Nezhdanov, D.V. Ershov, T.A. Guseinov, N.D. Gracheva, E.S. Malygin, Demidov, D.I. Tetelbaum, *Physics of the Solid State (St. Petersburg, Russia)* 54 (2012) 368.
- [21] S. Núñez-Sánchez, R. Serna, J. GarcíaLópez, A.K. Petford-Long, M. Tanase, B. Kabius, *Journal of Applied Physics* 105 (2009) 013118.
- [22] L. Bi, J.Y. Feng, *Journal of Luminescence* 121 (2006) 95.
- [23] I. Dogan, I. Yildiz, R. Turan, *Physica E* 41 (2009) 976.
- [24] N. Korsunskaya, T. Stara, V. Strelchuk, O. Kolomys, V. Kladko, A. Kuchuk, B. Romanyuk, O. Oberemok, J. Jedrzejewski, L. Khomenkova, I. Balberg, *Nanoscale Research Letters*, submitted for publication (ID: 1955309885820275).